Lock, R. J., Vaidyanathan, R., & Burgess, S. C. (2014). Impact of Marine Locomotion Constraints on a Bio-inspired Aerial-Aquatic Wing: Experimental Performance Verification. ASME Journal of Mechanisms and Robotics, 6(1), [011001]. DOI: 10.1115/1.4025471

Impact of Marine Locomotion Constraints on a Bio-inspired Aerial-Aquatic Wing: Experimental Performance Verification

This paper describes the design, fabrication, experimental testing and performance opti-mization of the morphology of a flapping wing for use on a robot capable of aerial and aquatic modes of locomotion. The focus of the optimization studies is that of wing design for aquatic propulsion. Inspiration for the research stems from numerous avian species which use a flapping wing for the dual purpose of locomotion (propulsion) in both air and water. The main aim of this research is to determine optimal kinematic parameters for marine locomotion that maximize nondimensionalized performance measures (e.g., propulsive efficiency), derived from analysis of avian wing morphing mechanisms that balance competing demands of both aerial and aquatic movement. Optimization of the ki-nematic parameters enables the direct comparison between outstretched (aerial) and retracted (aquatic) wing morphologies and permits trade-off studies in the design space for future robotic vehicles. Static foils representing the wing in both an extended and retracted orientation have been manufactured and subsequently subjected to testing over a range of kinematics. Details of the purpose built 2 degree-of-freedom (dof) flapping mechanism are presented. The gathered results enable validation of previously developed numerical models as well as quantifying achievable performance measures. This research focuses on the mechanical propulsive efficiencies and thrust coefficients as key performance measures whilst simultaneously considering the required mechanical input torques and the associated thrust produced. [DOI: 10.1115/1.4025471]

1 Introduction

Through the continuing miniaturization of mechatronic packages (e.g., sensors, electronics, and power storage), small robotic vehicles that would have once been infeasible to manufacture are emerging in the robotics community. Vehicles capable of aerial, terrestrial, and even aquatic locomotion are now showing increasing maturity in design. In addition, a greater understanding of animal locomotion has significantly improved the mobility and stability of these vehicles [1–3]. At this time, however, the challenges of robotic design for vehicles capable of locomotion through multiple media (e.g., air, water, land) have received less attention in robotic literature; while a few examples exist, including a preliminary study of the following research in conference proceedings (e.g., Refs. [4–9]), mechatronic design and control paradigms related to multiple modes of locomotion are not well established in robotic design. Robotic platforms capable of multi-modal locomotion may be broadly partitioned into one of two classes: those that use separate (independent) mechanisms for locomotion in different substrates, and those that employ dual-use mechanisms capable of altering morphology and/or control for locomotion through different media. For example, successful projects such as the morphing air-land vehicle [4], achieves aerial and terrestrial locomotion by using independent mechanisms on air and on land. While successful in achieving dual mode locomotion, this robot essentially required disparate mechanisms, sensors, and control systems for each locomotion mode. Conversely, the amphibious salamander robot [5] achieves this duality using a single mechanism, simplifying the complexity of the overall system. While trade-offs such as simplicity in design versus robustness and functionality potentially validate both approaches, we believe that drawing inspiration from avian species that utilize dual use mechanisms in air and water offers significant benefits in future vehicle designs. The design trade-offs involved between transitioning from aerial to aquatic locomotion modalities have yet to be addressed by the research community. Specific questions of interest include:

- How do mechanisms of locomotion and power distribution alter when considering robots with multiple modes of mobility?
- What are the benefits/costs involved in implementing dual use locomotion mechanisms versus separate means of mobility?
- Are there specific natural systems that may inspire specific solutions to the issues involved in multiple modes of locomotion?

1.1 Scope of Work.

We introduce and explore the premise that studying avian species that competently demonstrate both aerial and aquatic mobility utilizing a dual use propulsion mechanism will elucidate insights into the questions stated above, with the focus during this research on the aquatic capability of flapping foil propulsion utilizing a retracted wing. In keeping with these natural systems, we replicate the reduction in wing size during aquatic operations by implementing a retraction mechanism. This is due to the long term goal of developing a dual use flapping mechanism that could be used in both mediums in the same manner as the avian species.

Fig 1 Guillemot during aerial and aquatic locomotion (adapted from unpublished BBC footage) [15]

A known advantage of using flapping foil propulsion is the potential for highly maneuverable robot control. Flapping foil propulsion has been shown in several circumstances to enable hovering (e.g., Refs. [10,11]), a trait which opens up many potential applications. Future applications with respect to a robot capable of aerial and aquatic locomotion include the offshore oil industry, where the vehicle could fly from remote oil rigs, subsequently diving underwater to inspect pipe work and joints, environmental monitoring and exploration, littoral environment mine detection and maritime counter-terrorism operations where a boarding crew could launch a small robot to conduct both aerial and aquatic inspection/surveillance of a larger cargo ship. These are just some of the potential tasks that could be completed; the development of aerial/aquatic multi-modal vehicles would therefore represent a generational leap in robotic utility. The presented work details the development of the mechatronic system used to determine the performance of a retracted flapping wing used during aquatic locomotion and as a method of validating a numerical model of wing morphing to support future dual use wing designs capturing key features of the extended and retracted wing. Static foils representing a wing in these orientations have been fabricated and subjected to testing over a range of kinematic parameters, utilizing the purpose built mechatronic system (of which the design and development is detailed) capable of unconstrained controlled kinematics. The gathered results offer validation of a previously completed numerical model as well as showing achievable performances of a flapping foil, specifically the implications of the feasibility

of using a retracted wing; utilizing nondimensionalized performance measures to allow the findings to be scaled accordingly in future work.

2 Avian Inspiration

Within the domain of small robotic vehicles, natural systems still surpass man-made robotic systems in virtually every measure of performance. A case in point is the common guillemot, *Uria aalge*, a member of the auk family of seabirds, capable of flying distances as far as 30 km out to sea at an average velocity of 19 m/s, whilst also being able to swim proficiently underwater at an average speed of 1.5 m/s [12–14]. This transition from air to water leads to an approximate 800 times increase in fluid density. A key implication of this is the potential increase of profile drag forces experienced during the aquatic mode of operation. This helps explain why the guillemot folds in its wing during aquatic modes of locomotion, with the wing surface area reducing to approximately 58% of the fully extended shape used during aerial flight in order to reduce this drag contribution [15]. Additional consideration should also be given to the musculoskeletal system of the avian species, where by the retraction of the wing could be to increase wing rigidity which would be beneficial during high wing-loading during aquatic operations. As the guillemot's wings evolved initially for aerial flight, it is possible that they are retracted in the manner shown in Fig.1 in order to overlap the feather arrangement and provide a more rigid foil arrangement for aquatic operations, providing a more robust structure capable of operating in the denser aquatic environment. The kinematic viscosity of air is approximately 15 times greater than water. Therefore an object of a specific size will have the same Reynolds number in both mediums if the object was to travel 15 times faster in air, which the guillemot is observed to do [16]. Considering the stated average aerial and aquatic velocities it is interesting that the calculated operating Reynolds numbers for the guillemot was similar in both substrates, at approximately 70,000.

During aquatic operations, typical operating speeds reduce compared to aerial locomotion with the flapping frequency reducing from approximately 9 Hz to 2.5 Hz when moving from air to water; however, the Strouhal number, remains similar in each medium at approximately 0.18 in water and 0.19 in air. We believe that the selected aquatic flapping frequency is a limitation of the avian muscles, below which the muscle would be highly inefficient, leading to a requirement to reduce the wing into the body so that the muscle is sufficiently powerful to drive the reduced wing size at the required flapping frequency during aquatic operations. The capacity to shift morphology and movement between mediums obviously forces a performance compromise in functionality in each individually, which in the case of a natural system will be found through an evolutionary process. In order to establish and quantify these compromises, numerical modelling and empirical analysis is required to elucidate these trends.

3 Modeling

Several birds utilize a flapping technique underwater that develops lift on both the up and down stroke, which is then resolved into forward thrust, including species that are also capable of aerial operations [17]. This change in modality consistently sees the avian species retracting their wings inwards during aquatic operations and as such provides the main motivation behind the investigation of this mechanism, which aims to quantify the implications of this on overall multi-modal performance. The kinematic trajectory of the flapping foil arrangement was chosen to be similar to that of the adept avian swimmers of the auk family, utilizing a two degrees of freedom flapping motion consisting of roll, relating to the larger wing flapping action and pitch relating to the twisting action, operating in a harmonic manner with the same circular frequency x (rad/s). The relationship between the roll motion of the wing and the pitching motion can be considered to be as follows. First, the roll motion is governed by

(1) $$\varphi(t) = \varphi_0 \sin(\omega t)$$

where φ_0 is the maximum roll amplitude in radians. Similarly the pitch motion of the wing is governed by

(2) $$\theta(t) = \theta_o \sin(\omega t + \psi)$$

Where ϑ_0 is the maximum pitch amplitude in radians and ψ is the phase angle between pitch and roll. It has been highlighted in previous work that a phase lag of 90 deg is the most suitable arrangement which shall be adhered to here [18]. This results in Eq.(2) changing to

(3) $$\theta(t) = \theta_o \cos(\omega t)$$

Provided the maximum roll amplitude and pitching amplitude are known, the kinematics of the flapping foil are fully described, graphically shown in Fig. 2. It should be noted that during the flapping motion the effective angle of attack of the foil varies based on the local kinematics due to the resultant of the forward velocity and heave velocity due to the main flapping motion (i.e., roll motion) as shown in Eq.(4)

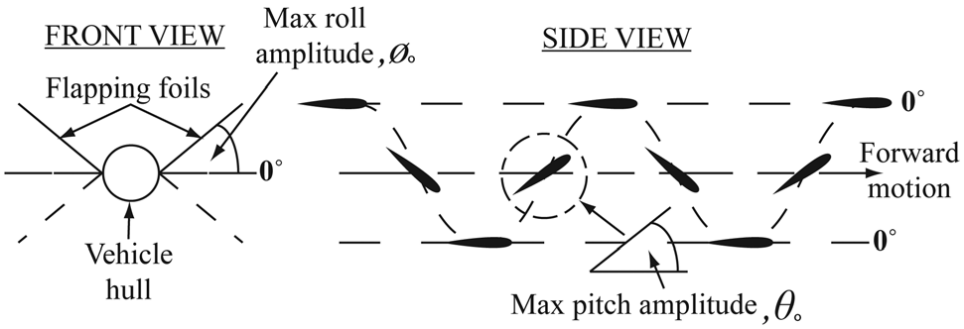

Fig. 2 Graphical representation of harmonic nature of the roll and pitch motions, demonstrating phase lag of maximum roll and pitch amplitude [15]

(4) $$\alpha(t) = \arctan\left(\frac{U_h}{U_f}\right) - \theta(t)$$

where $\alpha(t)$ is the effective angle of attack (deg), U_h is the heave velocity at the 70% span location (m/s) and U_f is the forward velocity (m/s).

4 Quantitative Performance Measures

Although the majority of underwater robotic vehicles rely on rotary propulsion, flapping wing approaches (in particular 2 dof structures similar to the swimming mode of the guillemot) have been the subject of several investigations in robotic literature (e.g., Refs. [10,19]). Similar flapping mechanisms have also been utilized in aerial modes of locomotion [20]. Where this research differs from the previous work is that the presented wing arrangement is designed to be utilized in both mediums, with the focus in this research on the aquatic mode, taking into consideration additional constraints associated with the aerial mode during this investigation. Initial numerical modeling of the system, combining inertial dynamics and hydrodynamics based on quasi-steady blade element theory, indicated that the use of a retracted wing that enabled a reduction in wing plan-form area could improve overall aerial/aquatic mission performance [21–23].

Static foils have been manufactured representing both the extended and retracted wing shapes and tested over a range of kinematic parameters, whilst recording key variables from within the system. From this gathered data consisting of torque measurements and thrusts generated, average power requirements, nondimensionalized mechanical propulsive efficiencies and thrust coefficients for each foil shape are determined.

The foil arrangements considered are as follows; first, the 2 degrees of freedom are arranged perpendicular to one another with a rectangular foil plan-form area, second, with the pitch axis mounted at 45 deg to the roll axis, the attached foil represents an equivalent wing to that of the initial rectangular plan-form area but which has been subjected to a retraction akin to a parallelogram and thirdly, an additional larger retracted wing whereby the span perpendicular to the roll axis is equivalent to the original rectangular foil so that direct comparisons can be made at equivalent kinematics and Strouhal numbers. These represent the two modes shown in the biological case in Fig. 1 which provided inspiration for the folding arrangement.
The equivalent models can be seen in Fig.3 which also details the proposed implementation of this retraction mechanism by means of a double four-bar mechanism that would enable the wing to fold in this manner. This mechanism will be developed fully in future work. All static models have the same chord length of 0.1 m and a symmetrical foil profile, described by a NACA 0012 profile. The equivalent foils have been fabricated so that they represent the same leading edge semi-span dimension of 0.35 m, matching that of the guillemot. The larger retracted model has a leading edge dimension of 0.5 m but a 0.35 m dimension in the purely span-wise direction, i.e., perpendicular to the roll axis. These dimensions include the attachment beam upon which the strain gauges are mounted.

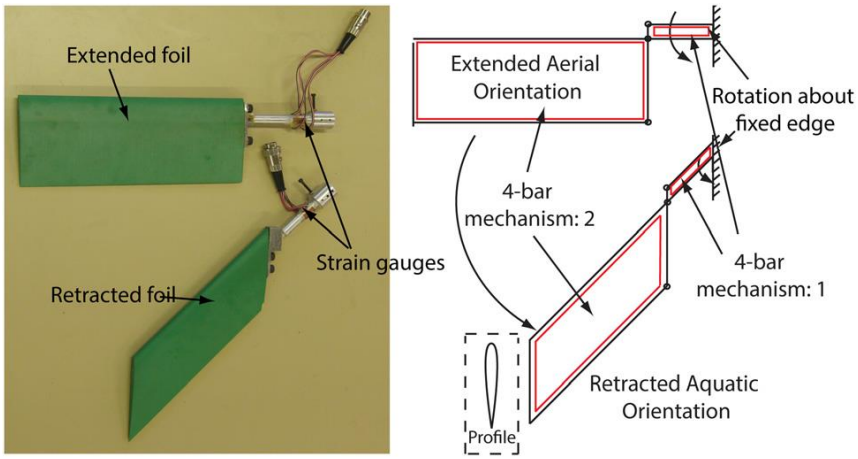

Fig. 3 Extended and retracted static foil modes with proposed four-bar mechanism to achieve wing morphing Journal of Mechanisms and Robotics

The mechanical propulsive efficiency is selected in order to isolate the mechanics of the system, meaning that the electrical losses associated with the inefficient reciprocating operation of the motors are not considered within the gathered results, enabling conclusions to be drawn relating to the specific performance of each foil shape and kinematic set rather than that of the actual driving mechanism. The mechanical propulsive efficiency is defined by the following ratio:

(5)
$$\eta_{\text{prop}} = \frac{\bar{P}_{\text{out}}}{\bar{P}_{\text{in}}}$$

where $\bar{P}_{\text{in}}$ represents the mechanical power into the system and $\bar{P}_{\text{out}}$ the useful mechanical power out of the system. The mechanical power into the system is determined by measuring the torques associated with each degree of freedom and then multiplying by the relevant angular velocities

(6)
$$P_i(t) = \tau_i(t) \cdot \omega_i(t)$$

where $P_i(t)$ is the power (W), $\tau_i(t)$ is the torque (Nm), and $\omega_i(t)$ the angular velocity (rad/s), all of which are time dependent. The i represents the degree of freedom in question. $\bar{P}_{\text{in}}$ is then calculated by determining the time averaged value for each degree of freedom and combining to give the overall value.

$\overline{P}_{out}$, representing the useful mechanical power out of the system is calculated based on the product of the generated thrust in the forward direction and the forward velocity in which the foil is traveling

(7) $$P_{out}(t) = F_x(t) \cdot U_f(t)$$

where $F_x(t)$ is the generated thrust (N) and $U_f(t)$ is the forward velocity (m/s). The time averaged value $\overline{P}_{out}$ is subsequently determined.
The thrust coefficient, C_t, is also determined to provide an additional performance measure. This is calculated by the following equation:

(8) $$C_t = \frac{\bar{F}_x}{1/2\rho U_f^2 A_{foil}}$$

where $\bar{F}_x$ is the time averaged thrust in the forward direction (N), ρ is the density of the water (kg/m^3) and A_{foil} is the surface area of the foil (m). The smaller retracted foil shape has a surface area of 63% of the extended wing. Utilizing Eq. (8) allows comparisons to be made between the different models taking into account this alteration in foils size.

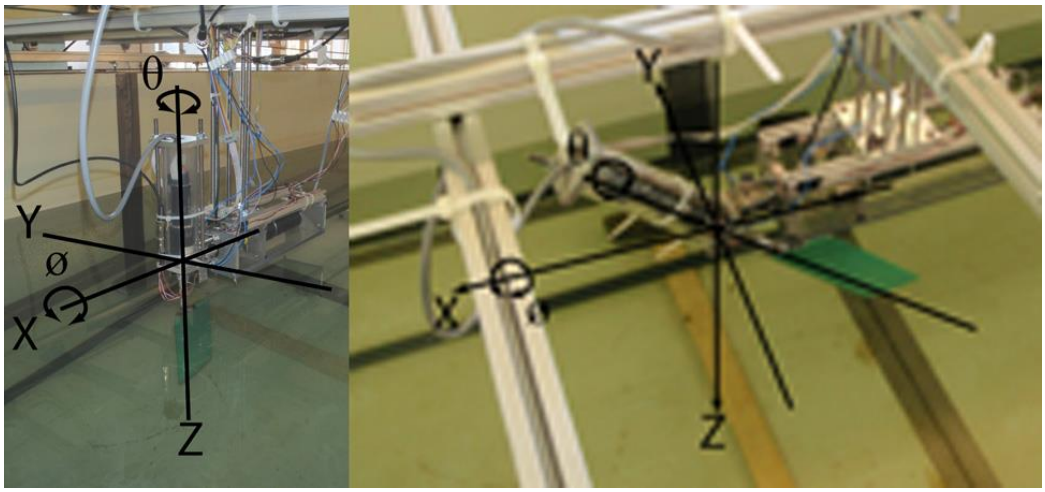

Fig. 4 Variation in pitch axis orientation (left: extended, right: retracted)

Although not strictly a performance measure, the Strouhal number, St, shall also be used when comparing the foil shapes. The Strouhal number is a dimensionless number that is used to describe oscillatory motion within fluids, relating the characteristic length and frequency of vortex shedding of the oscillating body with the velocity of the fluid

(9) $$St = \frac{fA}{U_f}$$

Where f is the frequency (Hz) and A is an estimate of the width of the wake associated with the flapping motion. This is approximated by calculating the amplitude of the foil taken at 70% span location based on the peak-to-peak roll amplitude, φ_0

(10) $$St = \frac{f(0.7b \sin \varphi_o)}{U_f}$$

where b is the wing semi-span length (m), measured perpendicularly from the roll axis. This dimensionless number is useful when comparing the various foil shapes, as the performance can be determined for each shape at equal St in order to elucidate similarities or differences in the

performance of each orientation, helping to establish the implications of the retracted position on vortex shedding.
Through a combination of the actual measured results combined with the nondimensionalized values, a clear picture of the implications of various kinematic changes can be determined for the different wing shapes.

5 Task Space Performance Measures

Although the quantitative performance measures in Sec. 4 allow detailed analysis of the system in question, additional consideration should also be given to task-space performance measures when considering a vehicle of this type. The environments in which the proposed vehicle will operate are highly dynamic in nature, such as countering waves during littoral tasks, strong currents when in open water or having to navigate in compact environments. It is therefore important to consider the impact of geometric variables such as foil size, and foil kinematics such as frequency on the likely obtainable performance.
Additionally, a major challenge for any multi-modal vehicle is the transition between mediums. Avian species are known to overcome this when plunge diving by retracting their wings backwards during impact [24]. The ability to retract the wings back on the current projected vehicle could be advantageous as a mechanism when entering water. This therefore provides additional task-space performance measures that need to be considered when analyzing the quantitative data:

- Preference for a compact foil design during aquatic mode of operation
- Flapping frequency high enough to enable control in a dynamically changing aquatic environment
- Ability to minimize vehicle frontal profile during transition from air to water

6 Mechatronic System

6.1 Flapping Foil Mechanism and Control.

The main requirement of the experimental arrangement stems from the ability to flap static foils whilst the 2 degrees of freedom are mounted perpendicular to one another or at 45 deg to one another as shown in Fig.4. This is achieved by allowing the connection terminal of the pitch and roll axes to be re-aligned depending on the arrangement under investigation.

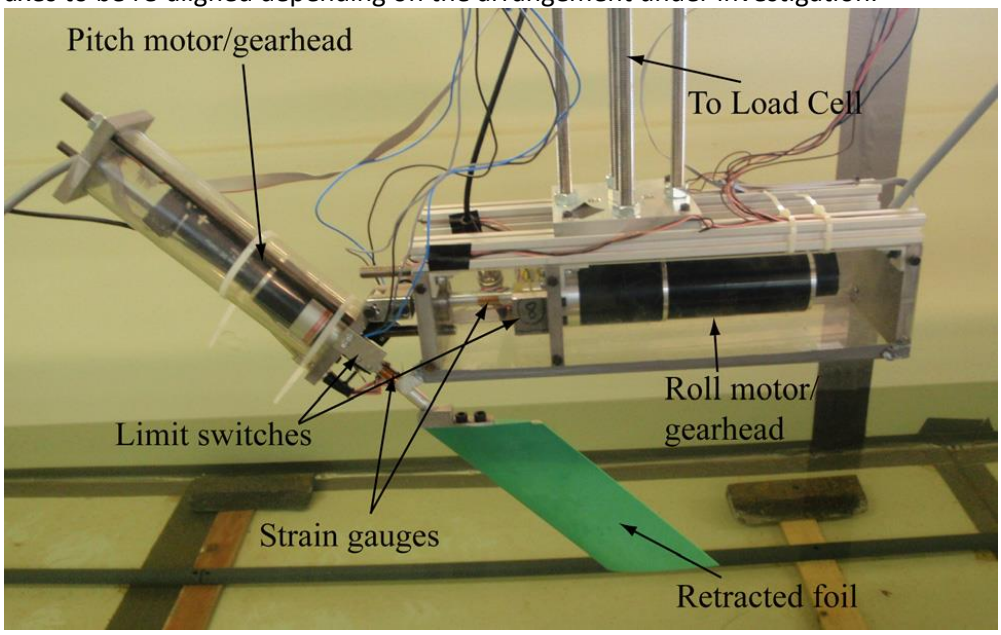

Fig. 5 Retracted flapping arrangement suspended below platform

A key aim of this research is to empirically determine whether similar propulsive efficiencies can be achieved for static wings mounted in the two arrangements shown in Fig.4. In order to be able to do

this over a large solution space, motors capable of driving each degree of freedom over a suitable range of kinematics are required. Through previous work, indications of the likely driving torques were presented which acted as a starting point for the motor specifications [21]. The selected motors for the roll and pitch degrees-of-freedom were a Maxon dc motor, type RE 50 (200 W) with a Maxon Planetary Gearhead type GP52 (53:1) and a Maxon dc motor, type RE 35 (90 W) with a Maxon Planetary Gearhead type GP42 (53:1). With the addition of the gearheads the motors are able to achieve the desired driving torques and with mechanical time constants of 4.2 and 5.97 ms, respectively, controlling the motors with the desired kinematic trajectories would be achievable. It should be noted that this arrangement was suitable for analyzing the aquatic phase and is not capable of the faster flapping frequencies associated with aerial locomotion.

As highlighted in Sec.4, the aim of this research is to identify trends relating to the mechanical propulsive efficiencies and thrust coefficients when varying foil orientation and shape, rather than investigating the efficiencies specific to the chosen implemented driving mechanism design. It must be stressed that the authors are not implying that the chosen arrangement of motors mounted and operated in this manner provides the most efficient method of achieving a 2 degree-of-freedom flapping mechanism, simply that this arrangement allows the investigation of a large search space whilst maintaining the quality of the results over the testing range. An additional method is therefore required to determine the mechanical torque for each degree of freedom.

Rosette strain gauges, Vishay type CEA-13-120CZ-120 were used to measure the torque in the shafts, set up in a full bridge arrangement and channeled through an amplifier and balance unit, Fylde types 254GA and 492BBS, respectively. The subsequent output voltages were then converted to digital signals via a National Instruments USB DAQ with the data being recorded using National Instruments LabVIEW 2010 to allow subsequent postprocessing.

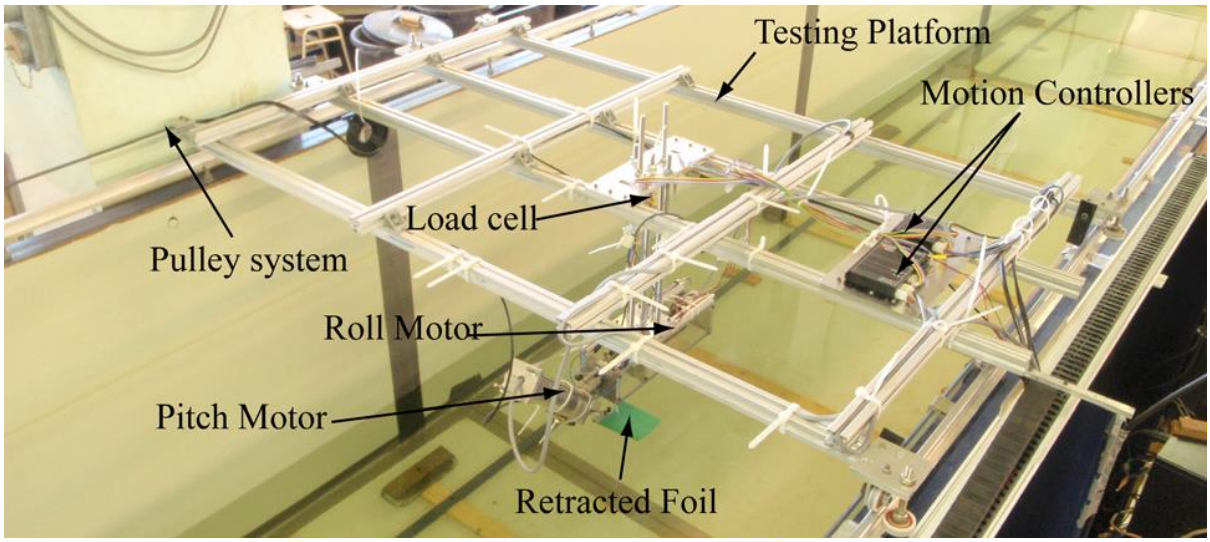

Fig. 6 Complete testing platform, flapping mechanism and control electronics

Strain gauges, Vishay type EA-13-240LZ-120/E, mounted to the support beam below the platform were used to quantify the amount of thrust generated by the flapping motion, again set up in a full bridge arrangement. The load cell is highlighted in Fig.6, the position of which was adjusted for the various wing orientations in order to minimize the moment arm between the load-cell and flapping motion.

During measurements utilizing the strain gauges, it should be noted that the percentage error of the outputs, determined through preliminary calibration, was found to be significant at low recorded values of thrust and torque ($F_x \leq 0.25$ N; $\tau_i \leq 0{:}1$ Nm) experiencing errors >10% in certain cases. Above these values, average % error was calculated as 6.28%, 5.27%, and 2.38% for the thrust, roll torque and pitch torque measurements, respectively.

To achieve the required motions, Maxon EPOS 70/10 motioncontroller units were utilized. The motion controllers implement on-board proportional-integral-derivative (PID) control strategies. Velocity control was selected as the control strategy for the motion. The command signals required by the motion control units were sent via serial (RS232) communication. The overall flapping arrangement, suspended below the testing platform can be seen in Figs. 5 and 6.

6.2 Aquatic Testing Environment and Dynamic Testing Platform.

Based on how the mechanical propulsive efficiency is calculated a known, constant forward velocity of the carriage is required so that the amount of useful mechanical power out of the system can be quantified. In order to achieve this, a movable carriage suspended above a water tank has been developed. The overall dimensions of the water tank are 15 x 1.5 x 1.6 m, of which the actual test runs cover a horizontal distance of 10.5 m. This length was selected due to the implementation of required safety features at the extremities of the projected motion, whereby limit switches were hardwired into the driving electronics to ensure the rig did not exceed the maximum permissible motion. The carriage was constructed from bespoke lengths of aluminum profile sections. The completed platform can be seen in Fig. 6.

In order to control the motion of the platform, a continuous drive belt was connected to the platform via a free spinning pulley at one end of the tank, and another connected to a pulley directly connected to a dc motor.

The dc motor, a Parvalux type PM4C 24 V þ MB Gearhead, was controlled via an additional motion controller. A HEDS 5540 encoder was connected to the shaft of the motor, with the digital encoder signal being fed back through the same NI DAQ 6211 card. This ensured that accurate measurements of platform speed were used during post-processing.

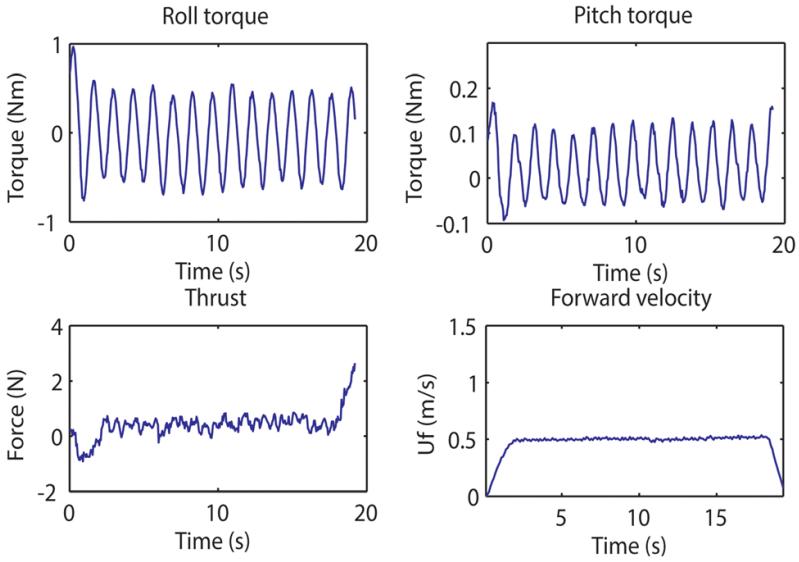

Fig. 7 Complete data set for individual test run (retracted wing, $\varphi_o = 40$ deg, $\theta_o = 30$ deg, $f = 0.75$ Hz, and $U_t = 0.5$ m/s

6.3 Overall Experimental Control Interface.

To complete the synergy of mechanics and electronics, the entire operation was controlled through a purpose built user interface within the National Instruments software package LabVIEW 2010. This environment was designed in a manner so that all the variables could be set according to the desired kinematics, controlling the flapping foil motion and the velocity of the towing platform whilst simultaneously gathering data relating to the torques experienced in the shafts, the thrust generated by the flapping arrangement and then compiling the entire data set relating to the time dependent values of the various foil kinematics and recorded inputs. At each test run a *.csv file was

exported and saved for post processing. The interface was designed in such a manner that once the amplitude and frequency of the roll and pitch motions were specified in the front panel, the velocity trajectories required by each motor were determined with these time dependent values subsequently sent as commands to the EPOS motion controllers via the serial (RS232) communications.

7 Results

The effects of maximum roll and pitch amplitudes on the output performance are initially presented, at a flapping frequency of 1.0 Hz and a forward velocity set at 0.5 m/s for the equivalent extended and retracted foil profiles. This data allows the direct comparison of performance of what would be considered the same wing, in the larger extended orientation and then the smaller retracted orientation. The maximum roll amplitude was varied between 20 deg and 40 deg, and the pitch between 10deg and 30deg at increments of 5 deg. Each parameter set was tested a minimum of 5 times, outputting a data set as described in Sec. 6.3. An example of a typical complete data set for one run can be seen in Fig.7. The effects of forward velocity, flapping frequency and subsequently Strouhal number were also investigated, comparing the extended foil and larger retracted foil so that direct comparisons could be made when using the same kinematic variables. When varying the forward velocity, the flapping amplitude was fixed at 40 deg and the flapping frequency adjusted so that discrete Strouhal numbers were achieved, governed by Eq. (10), ranging from 0.17 to 1.51 Hz. These were then tested over a range of effective angles of attack and plotted in a continuous manner. Post-processing of the results was carried out in Matlab 2009b (Mathworks, Inc.). As the aim was to determine the torques associated with the flapping motion, a technique was required in order to eliminate the torque associated with oscillating the pitch motor, mounted as shown in Fig. 6. In order to eliminate the need to complete test runs without the foils attached to determine these values, the torque was calculated numerically and subtracted from gathered results. To do this, an equation of motion for the pitch motor about the roll axis was determined as follows:

(11) $$I_{\theta-\text{motor}}\underline{\alpha}_X + g(\eta) = \tau_{\theta-\text{motor}}$$

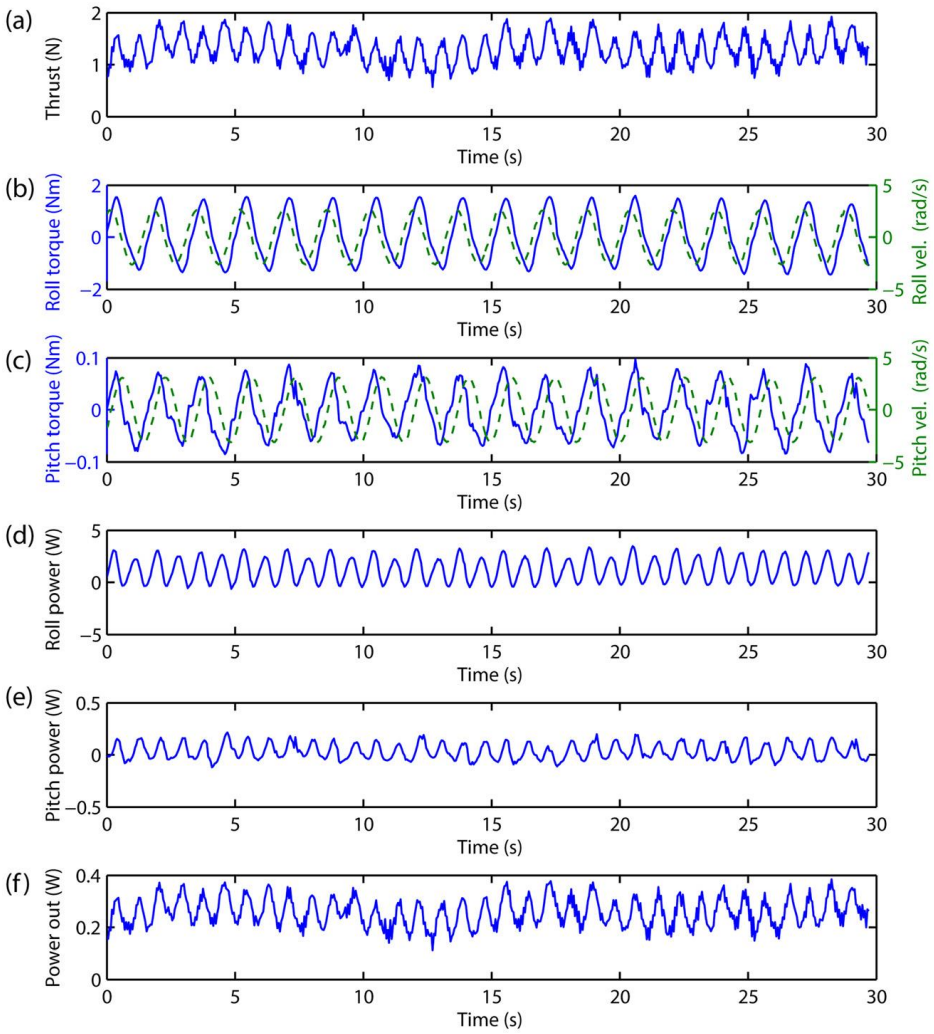

Fig. 8 Reduced data set for individual test run (retracted wing, $\varphi_o = 40$ deg, $\theta_o = 30$ deg, $f = 0.75$ Hz, and $U_f = 0.5$ m/s). Plots (*a*) and (*b*): Solid line—torque, dashed line—angular velocity

Where $I_{\vartheta\text{-motor}}$ is the inertia tensor associated with the pitch motor and casing, $\underline{\alpha}_x$ is the acceleration about the roll axis (i.e., X-axis), g*(η)* is the vector of gravitational forces and moments and $\tau_{\vartheta\text{-motor}}$ is the subsequent torque associated with the pitch motor and casing. The inertia tensor was modified depending on whether the pitch motor was mounted vertically or in the retracted orientation.
To determine the average values based on the repeated runs the data sets were partitioned so that the periods of platform acceleration and deceleration were eliminated. An example of this data can be seen in Fig. 8. Time averaged values were then calculated as detailed in Sec. 4.

7.1 Numerical Model Validation.
Using a numeric model to simulate empirical testing enabled the development of a large solution space, investigating the implications of alterations in geometry as well as kinematics [21]. The aim was that if the model matched the empirical results for the extended and retracted foil shapes presented, the numerical model could be utilized in future work with an elevated degree of confidence in the outputted values and eliminate the need to manufacture many different foil sizes in order to determine an equivalent solution space.
A comparison of the predicted and recorded values for the extended wing shape can be seen in Fig. 9. It can be seen that there are differences in these results for this kinematic set.

Beginning with the thrust measurement, it appears that the recorded value experiences high frequency noise, which the authors believe to be a result of the vibration of the dynamic platform as it runs along the rails. Future work aims to introduce a smoother running platform to eliminate this. The strain gauges used will also be subject to the anticipated % error in measured value achievable by the selected gauges at these low values of thrust measurement. Additional error could also stem from the fact that the lift coefficient value used in the numerical modelling does not account for variations in Re number and as a result could lead to further errors in numerically determined thrust values.

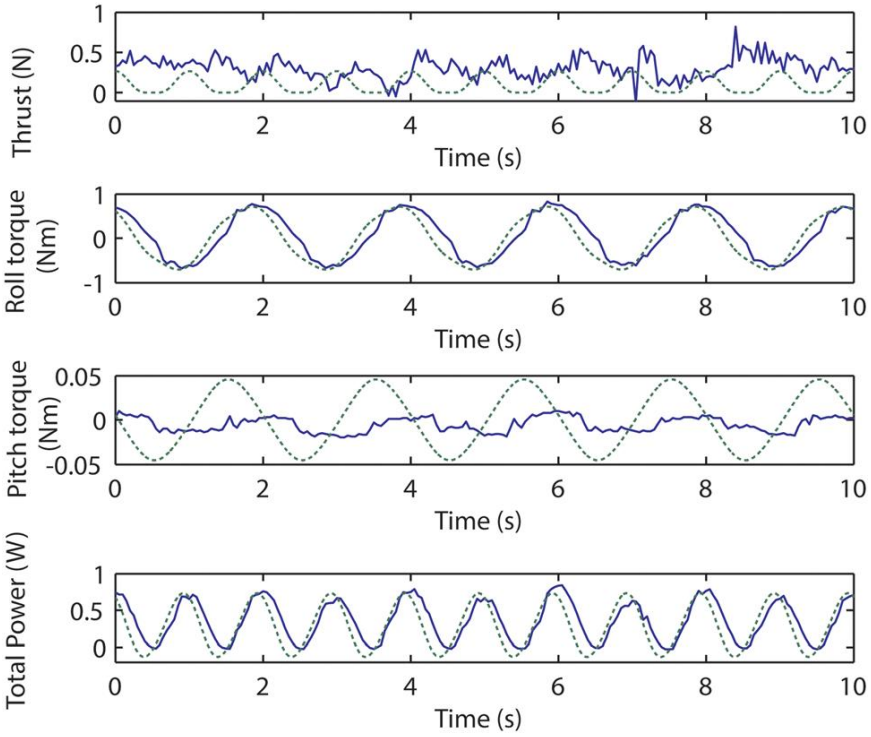

Fig. 9 Comparison of predicted and measured values for the extended foil shape solid line and dashed line, respectively ($\varphi_o = 20$ deg, $\theta_o = 15$ deg, $f = 0.5$ Hz, and $U_t = 0.25$ m/s)

Table 1 Comparison of measured (Emp.) and predicted (Num.) values for extended and retracted foil shapes

	Case 1			Case 2		
Extended	Emp.	Num.	% error	Emp.	Num.	% error
Thrust (N)	0.31	0.10	−66.3	2.66	1.98	−25.5
τ_{roll}	0.83	0.71	−13.9	1.95	4.23	117.5
Max roll power (W)	0.84	0.74	−12.7	5.69	12.8	125.0
Average power (W)	0.36	0.29	−19.0	2.05	5.09	147.9
	Case 3			Case 4		
Retracted	Emp.	Num.	% error	Emp.	Num.	% error
Thrust (N)	0.68	0.72	7.0	0.16	0.08	−47.2
τ_{roll}	0.85	1.06	24.7	0.61	0.84	37.7
Max roll power (W)	3.15	3.71	17.7	1.69	2.14	26.5
Average power (W)	1.04	1.11	6.8	0.68	0.75	9.9

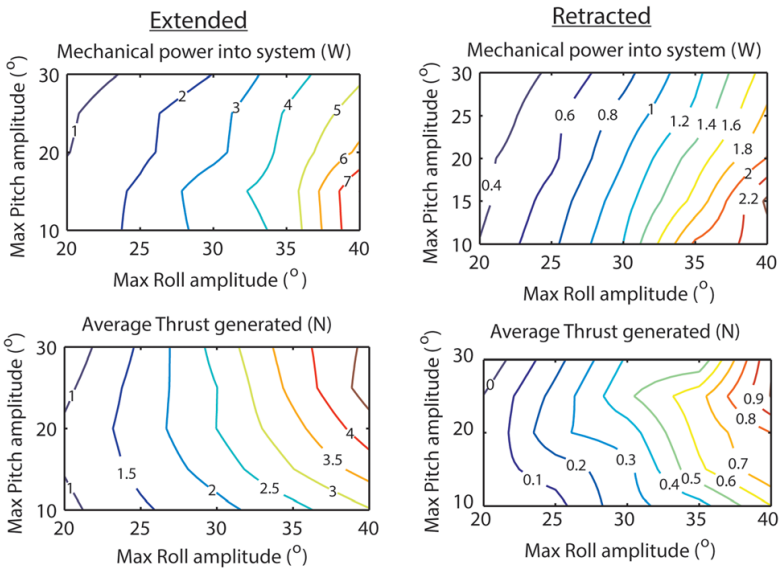

Fig. 10 Performance maps of extended and retracted foil orientation ($f = 1$ Hz, $U_f = 0.5$ m/s)

The empirically measured and numerically determined pitch torque and power values were consistently different. This is the result of two different issues. First, at low measurements of torque, the % error of the strain gauges used will have implications on the accuracy of the results, as discussed in Sec.6.1. Second, it appears that at certain selected kinematic sets, the roll torque appears to dominate the measured values. It can be seen that the recorded value for the pitch torque is in phase with the roll torque, which from initial numerical modeling should not be the case. This is due to the coupling of the pitch and roll torques, which cannot be separate with the current transducer arrangement. It can be noted, however, that for all kinematic sets, the roll torque always dominates and as such constitutes the greater part on the overall flapping motion power requirement.

The correlation of the numerical and empirical results varied for different kinematic sets as shown in Table 1. For the extended values, case 1 is tested at $\varphi_0 = 20$ deg, $\vartheta_0 = 15$ deg, $f = 0.5$Hz, and $U_f = 0.25$ m/s and case 2 at $\varphi_0 = 30$ deg, $\vartheta_0 = 30$ deg, $f = 1$ Hz, and $U_f = 0.5$ m/s. For the retracted case 3 is $\varphi_0 = 35$ deg, $\vartheta_0 = 30$ deg, $f = 1$ Hz, and $U_f = 0.5$ m/s and case 4 is $\varphi_0 = 25$ deg, $\vartheta_0 = 15$ deg, $f = 0.5$ Hz, and $U_f = 0.5$ m/s. It can be seen from these results that the error between the numerical model and the empirical values varied for different test sets. It was noted that in general the numerical model predicted a lower value for thrust generation than the actual measured values.

These errors have led the authors to reconsider parameters and assumptions made within this model, particularly the manner in which the lift coefficient was modeled over the course of the flapping motion, which did not adjust according to Re number. Adjustments in this modeling strategy shall be investigated in future work. At this time, however, the numerical model can still be used as a preliminary design aid, as the predicted values are typically higher in the numerical model and as such adhering to these values in subsequent design work will introduce a factor of safety within the range of 1.2–2 due to this over estimation, dependent on the kinematic conditions.

7.2 Equivalent Wing Size Analysis.

A comparison of the power requirements and thrust generation tested at the same kinematics can be seen for the equivalent extended and retracted wings in Fig. 10. It can be seen that the retracted wing requires less power than the extended wing, as would be expected with the reduction in foil surface area associated with this orientation. In general the mechanical power into the system for the retracted foil is approximately a 1=4 of that of the extended wing. However, the thrust generated also reduces, with the thrust produced by the retracted wing being as low as 15% of that generated by the extended wing at equivalent kinematic values. Similarly to the reduction in

mechanical power into the system, this comes as no surprise considering the reduction in surface area. A compromise in performance is present, whereby the retracted foil clearly requires less power but this comes at a subsequent loss in thrust production. It should also be noted that although not shown, η_{prop} and C_t were observed to be lower for the retracted wing highlighting the importance of optimal kinematic selection if a retracted wing was to be used.

7.3 Foil Shape Performance Comparison.

To make direct performance comparisons between foil shapes, the local kinematics experienced by each foil must be standardized. Manufacturing the larger retracted wing, as described in Sec. 4, enabled testing at equivalent St values and max a, allowing direct comparisons to be made between the performance of the extended and retracted profiles. These results are presented for the retracted and extended foil in Figs. 11and 12, respectively. For each performance map the roll amplitude and forward velocity is constant, with the flapping frequency adjusted so that the testing could be performed at discrete Strouhal numbers. These flapping frequencies varied from $f \approx 0.12$ Hz at a forward velocity of 0.2 m/s and a St = 0.2, up to $f \approx 1.2$ Hz at a forward velocity of 0.4 m/s and St = 1.0.

Overall, the mechanical power required and thrust generated increases with increasing Strouhal number for both foil shapes. Another observed trend is that as the forward velocity increases, power requirements increase at equivalent Strouhal numbers, with this trend observed for both foils. Similarly, at equal Strouhal numbers, the thrust produced increases with an increase in velocity. However, C_t, although increasing with St number, can be seen to be comparable at the different forward velocities for both foil shapes.

However, of greatest interest are the achievable propulsive efficiencies. It can be seen that both the extended and retracted foils perform poorly at the low forward velocity, indicating the unsuitability of flapping foils as an efficient means of propulsion at speeds $\leq$0.2 m/s. This can be explained by the fact that the performance of the NACA0012 profile depends on the operating Reynolds number. It has been shown that the maximum lift coefficient of the NACA0012 profile increases with increasing Re, therefore leading to a potential improvement in performance [25]. At the slow speed the Re range was calculated as ≈32,000–130,000 whereas at the faster velocity, this range increased to ≈65,000–260,000, leading to the observed increase in foil profile performance. As the forward velocity increases, a steady increase in η_{prop} is observed with increasing St, with the point of greatest interest being that the propulsive efficiencies for the extended and retracted foils are comparable over the range of St. This therefore demonstrates that a retracted wing can be used in place of an extended foil as a means of aquatic propulsion due to its comparable performance, provided the chosen kinematics are carefully selected.

7.4 Aquatic Vehicle Feasibility.

Ultimately the magnitude of the generated thrust needs to be equal and opposite in direction to the drag associated with the nonforce producing appendages to allow constant forward motion. This drag component is referred to as the parasitic drag. As this research is investigating the feasibility of utilizing a retracted wing in this manner, it would be of use to test the suitability of vehicle propulsion using the retracted foil. To do this, we begin with Eq. (12) relating to parasitic drag

(12) $$D_{par} = 1/2\,\rho U_f^2 A_{sw} C_d$$

where D_{par} is the parasitic drag (N), A_{sw} is the wetted surface area (m^2) and C_d is the drag coefficient. Remaining with the inspiration for the current robot stemming from birds with this capability, a drag coefficient calculated from a static model of a guillemot body can be used in Eq. (12) [26], taking into consideration the variation of Reynolds number on this coefficient. The shape of the fuselage is estimated as a prolate spheroid with a ratio of 6:1, with the equatorial radius fixed at 0.05 m and the polar radius set at 0.3 m, resulting in a 0.6 m overall vehicle length and a surface area of

approximately 0.15 m^2. The generated thrust by the retracted foil, in this case taken from the larger retracted foil, has to counter the parasitic drag at various forward velocities. The associated power requirement involved in generating this can then also be determined. Table 2 details the values calculated for three forward velocities where Re and C d relate to the vehicle fuselage.

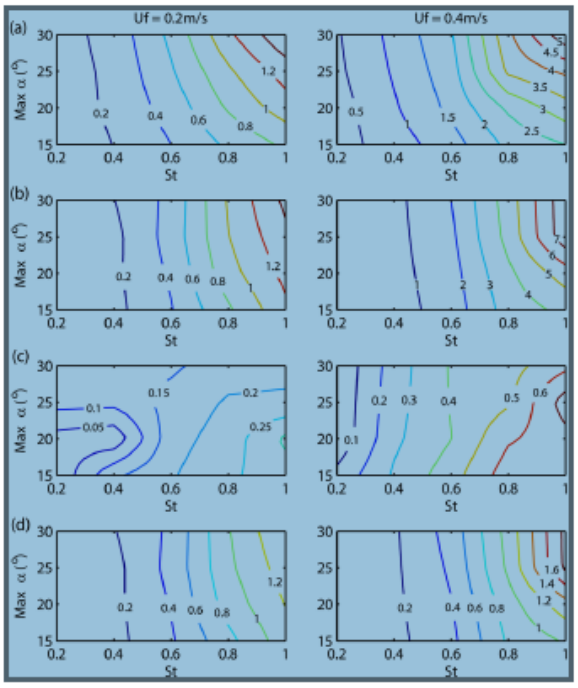

Fig. 11 Performance maps of retracted foil orientation. (*a*) Average power (W), (*b*) average thrust (N), (*c*) η_{eff}, and (*d*) C_t. Column 1—$U_f = 0.2$ m/s, column 2—$U_f = 0.4$ m/s, $\varphi_o = 40$ deg, frequency varied according to St number

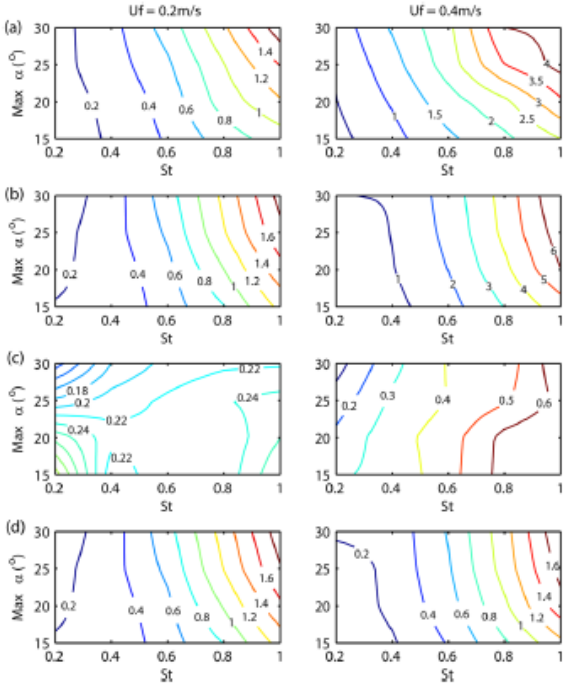

Fig. 12 Performance maps of extended foil orientation. (*a*) Average power (W), (*b*) average thrust (N), (*c*) η_{eff} and (*d*) C_t. Column 1—$U_f = 0.2$ m/s, column 2—$U_f = 0.4$ m/s, $\varphi_o = 40$ deg, frequency varied according to St number

Table 2 Projected achievable mission lengths for hypothetical vehicle (fuselage-prolate spheroid, 0.1 × 0.6 m)

Vel (m/s)	Re ($\times 10^3$)	C_d [26]	D_{par} (N)	Average power (W)	η_{eff}	Time (h)
0.2	60	0.06	0.36	0.56	0.14	10.7
0.4	120	0.045	1.08	1.534	0.31	3.9
0.6	180	0.038	2.025	4.225	0.59	1.4

Potential mission time lengths associated with using a retracted foil can then be estimated if the overall vehicle system is considered as displayed in Fig. 13. Based on the vehicle's proposed multi-modal capability, overall mass limitation is paramount. For this reason, the total mass designated to power supply has been estimated as 0.25 kg. Based on utilizing a lithium-ion polymer battery, this translates to a potential of 37.5 Wh [27], subsequently halved to account for power requirements in air and water, with a further 7.5 W allocated to on-board payload power draw.

Inputting efficiencies relating to the actuator mechanism, in this case consisting of a dc motor and gearhead [28], and hypothetical mechanism transmission efficiencies, an estimate of the overall time length is determined. The results are presented within Table 2. It must be stressed that this estimate does not take into consideration inefficient operations at other velocities. It should also be noted that the power requirements during this analysis use the values with the torque component for the pitch motor removed as discussed in Sec. 6.3. This is based on the assumption that the final vehicle will operate with a more compact mechanical flapping mechanism and as such additional

power requirements associated with this motion are accounted for within the mechanical transmission efficiency.

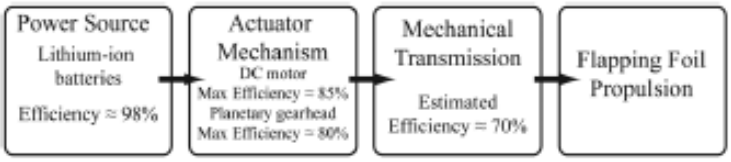

Fig. 13 Vehicle energy flow diagram [27,28]

Using a retracted foil in this manner does have potential and when considering additional design constraints such as the requirement to minimize overall mass of the vehicle, the implications that the reduced foil requires less power to flap essentially means that a smaller driving mechanism would be required to generate the flapping motion. This would certainly help in minimizing the overall vehicle size, and enable the use of a larger wing during aerial operations and then retract it in this manner during aquatic locomotion.

Directly comparing the performance of the flapping foil propulsion mechanism (estimated motor system efficiency: 47%, maximum propulsive efficiency: 70%) with traditional propeller driven mechanisms (motor efficiency: 66%, propeller efficiency: 80% [29]) indicates that with careful design of the mechanical transmission and selection of kinematics, overall system performance can be competitive.

The authors stress the fact that the presented results represent a subset of actual potential operating kinematics. As shown in Ref. [21], the optimal kinematic parameters to use vary for all combinations of mission requirements. It is therefore the authors' aim to continue investigations into the implications of kinematic variations in an attempt to develop a more complete solution space.

8 Conclusion

This research has begun to quantify the challenges in maximizing locomotive efficiency through multiple media, with specific focus on aquatic/aerial substrates. To our knowledge it is the first work quantifying the trade-offs and difficulties in this area and is envisioned to serve as a foundation for future vehicles capable of aerial and aquatic locomotion. There are several key differences between the presented research and the studied natural system, particularly the difference in the range in optimal St the natural and engineered systems appear to operate. We believe, however, that broader parallels in morphology shift, flapping oscillation, and performance optimization, support continued study of flapping mechanisms as a means of propulsion in both air and water that will, in the future, lead to the development of an aerial/aquatic vehicle.

The conclusions that can be drawn from the presented research relating to the feasibility of using a retracted wing as a means of propulsion during aquatic operations are:

- Given the demonstrated thrust generation, the use of a retracted foil is a feasible flapping foil propulsion mechanism
- Utilizing a driving mechanism that can achieve operations atSt0.8 will maximize performance of the retracted foil profile
- Aquatic mission lengths of 1.4–10.7 h shown to be achievable utilizing retracted foil
- The swept back foil profile reduces the required power to drive the motion to approximately a 1=4 of the equivalent extended foil profile for the same kinematic conditions, but this comes with a reduction in thrust production
- At equivalent Strouhal numbers, the retracted foil achieves the same level of propulsive efficiency and thrust coefficient values as the extended orientation
- Increasing flapping frequency demonstrated an improvement in foil performance, useful when considering the task-space performance measures

- Flapping foil propulsion, either with an extended or retracted wing, is inefficient at slow speeds ($\leq$0.2 m/s)
- Numerical model validated as potential design tool, due to tendency to over-estimate values hence introducing a factor of safety prior to actual design.

In future work flexible foils shall also be investigated to try to establish the role of coupling between neuromechanics and control stability in morphing structures adapting to locomotion transfer. Additionally, investigations into the synergy of the findings relating to mechanical propulsive efficiencies and potential compact driving mechanisms and associated electric efficiencies shall be completed in order to develop a clearer foundation for the mechatronic development of a prototype vehicle.

Acknowledgment
The authors acknowledge the support of the UK Engineering and Physical Sciences Research Council (EPSRC) Doctoral Training Assistantship (DTA) Program. We also express our gratitude to Capt (ret.) Jeffery E. Kline at the US Naval Postgraduate School for mission and utility insights.

References
[1] McIntosh, S. H., Agrawal, S. K., and Khan, Z., 2006, "Design of a Mechanism for Biaxial Rotation of a Wing for a Hovering Vehicle," IEEE/ASME Trans. Mech., 11(2), pp. 145–153.
[2] Granosik, G., 2005, "Integrated Joint Actuator for Serpentine Robots," IEEE/ ASME Trans. Mech., 10(5), pp. 473–481.
[3] Liu, F., Lee, K., and Yang, C., 2011, "Hydrodynamics of an Undulating Fin for a Wave-Like Locomotion System Design," IEEE/ASME Trans. Mech., pp.1–9.
[4] Bachmann, R. J., Boria, F. J., Vaidyanathan, R., Ifju, P. G., and Quinn, R. D., 2009, "A Biologically Inspired Micro-Vehicle Capable of Aerial and Terrestrial Locomotion," Mech. Mach. Theory, 44(3), pp. 513–526.
[5] Ijspeert, A. J., Crespi, A., Ryczko, D., and Cabelguen, J., 2007, "From Swimming to Walking With a Salamander Robot Driven by a Spinal Cord Model,"Science, 315(5817), pp. 1416–1420.
[6] Kovacˇ, M., Germann, J., Hurzeler, C., Siegwart, R. Y., and Floreano, D., 2010, € "A Perching Mechanism for Micro Aerial Vehicles," J. Micro-Nano Mech., 5(3–4), pp. 77–91.
[7] Georgiades, C., German, A., and Hogue, A., 2004, "AQUA: An Aquatic Walking Robot," IEEE/RSJ International Conference on Intelligent Robots and Systems, pp. 3525–3531.
[8] Harkins, R., Dunbar, T., Boxerbaum, A. S., Bachmann, R. J., Quinn, R. D., Burgess, S. C., and Vaidyanathan, R., 2009, "Confluence of Active and Passive Control Mechanisms Enabling Autonomy and Terrain Adaptability for Robots in Variable Environments," IAENG Transactions on Electrical and Electronics Engineering, Vol. I, 138–149.
[9] Lock, R. J., Vaidyanathan, R., and Burgess, S. C., 2012, "Design and Experimental Verification of a Biologically Inspired," IEEE International Conference on Biomedical Robotics and Biomechatronics, pp. 681–689.
[10] Licht, S., Hover, F., and Triantafyllou, M. S., 2004, "Design of a Flapping Foil Underwater Vehicle," IEEE J. Ocean. Eng., 21(3), pp. 311–316.
[11] Georgiades, C., Nahon, M., and Buehler, M., 2009, "Simulation of an Underwater Hexapod Robot," Ocean Eng.,36(1), pp. 39–47.
[12] Gaston, A. J., 1998, The Auks: Bird Families of the World, Oxford University Press, Oxford, UK.
[13] Lovvorn, J. R., Croll, D. A., and Liggins, G. A., 1999, "Mechanical versus Physiological Determinants of Swimming Speeds in Diving Brunnich's € Guillemots," J. Exp. Biol., 202, pp. 1741–1752.
[14] Pennycuick, C. J., 1987, "Flight of Auks (Alcidae) and Other Northern Seabirds Compared With Southern Procellariiformes: Ornithodolite Observations," J. Exp. Biol., 128, pp. 335–347.
[15] Lock, R. J., Vaidyanathan, R., Burgess, S. C., and Loveless, J., 2010, Development of a Biologically Inspired Multi-Modal Wing Model for Aerial-Aquatic Robotic Vehicles Through Empirical and

Numerical Modelling of the Common Guillemot, Uria Aalge,"Bioinspiration Biomimetics,5(4), pp. 1–16.
[16] Vogel, S., 1996, Life in Moving Fluids, Princeton University Press, Princeton, NJ.
[17] Johansson, L. C., 2002, "Kinematics of Diving Atlantic Puffins (Fratercula arctica L.): Evidence for an Active Upstroke," J. Exp. Biol., 205, pp. 371–378.
[18] Read, D., 2003, "Forces on Oscillating Foils for Propulsion and Maneuvering,"J. Fluids Struct., 17(1), pp. 163–183.
[19] Beal, D. N., and Bandyopadhyay, P. R., 2007, "A Harmonic Model of Hydro-dynamic Forces Produced by a Flapping Fin," Exp. Fluids, 43(5), pp. 675–682.
[20] Madangopal, R., and Agrawal, S. K., 2006, "Energetics-Based Design of Small Flapping-Wing Micro Air Vehicles," IEEE/ASME Trans. Mech., 11(4), pp. 433–438.
[21] Lock, R. J., Vaidyanathan, R., and Burgess, S. C., 2010, "Development of a Biologically Inspired Multi-Modal Wing Model for Aerial-Aquatic Robotic Vehicles," IEEE International Conference on Intelligent Robots and Systems, pp. 3404–3409.
[22] Lock, R. J., Vaidyanathan, R., and Burgess, S. C., 2010, "Mission Based Optimization of a Biologically Inspired Multi-Modal Wing Model for Aerial-Aquatic Robotic Vehicles," 11th Conference—Towards Autonomous Robotic Systems, Plymouth, UK, pp. 140–147. Available at: http://www.tech.plym.ac.uk/soc/staff/guidbugm/taros2010/slides/Lock%20-%20TAROS%202010.pdf
[23] Techet, A. H., 2008, "Propulsive Performance of Biologically Inspired Flapping Foils at High Reynolds Numbers," J. Exp. Biol., 211(Pt 2), pp. 274–279.
[24] Nelson, B., 1978, The Gannet, T. & A.D. Poyser Ltd., Hertfordshire, UK.
[25] Abbott, I. H., and Von Doenhoff, A. E., 1959, Theory of Wing Sections, Dover Publications, Inc., New York.
[26] Lovvorn, J., Liggins, G. A., Borstad, M. H., Calisal, S. M., and Mikkelsen, J., 2001, "Hydrodynamic Drag of Diving Birds: Effects of Body Size, Body Shape and Feathers at Steady Speeds," J. Exp. Biol., 204, pp. 1547–1557.
[27] Tarascon, J. M., and Armand, M., 2001, "Issues and Challenges Facing Rechargeable Lithium Batteries," Nature, 414(6861), pp. 359–367.
[28] Available at: http://www.maxonmotor.com
[29] Bellingham, J. G., Zhang, Y., Kerwin, J. E., Erikson, J., Hobson, B., Kieft, B., Godin, M., et al., 2010, Efficient Propulsion for the Tethys Long-Range Autonomous Underwater Vehicle," 2010 IEEE/OES Autonomous Underwater Vehicles, IEEE, pp. 1–7.

Richard J. Lock
Faculty of Engineering,
University of Bristol,
Bristol BS8 1TR, UK
e-mail: Richard.lock@bristol.ac.uk

Ravi Vaidyanathan
Senior Lecturer in Bio-mechatronics,
Imperial College London,
London SW7 2AZ, UK
e-mail: r.vaidyanathan@imperial.ac.uk

Stuart C. Burgess
Professor of Engineering Design,
Faculty of Engineering,
University of Bristol
Bristol BS8 1TR, UK
e-mail: s.c.burgess@bristol.ac.uk